Radiology

REVIEWS AND COMMENTARY • REVIEW

Hyperpolarized ^{13}C MRI: State of the Art and Future Directions

Zhen J. Wang, MD • Michael A. Ohliger, MD, PhD • Peder E. Z. Larson, PhD • Jeremy W. Gordon, PhD • Robert A. Bok, MD, PhD • James Slater, PhD • Javier E. Villanueva-Meyer, MD • Christopher P. Hess, MD, PhD • John Kurhanewicz, PhD • Daniel B. Vigneron, PhD

From the Department of Radiology and Biomedical Imaging, University of California San Francisco, San Francisco, CA 94143. Received October 25, 2018; revision requested November 24; final revision received January 5, 2019; accepted January 9. **Address correspondence to** Z.J.W. (e-mail: *Zhen.Wang@ucsf.edu*).

Supported by the National Institute of Biomedical Imaging and Bioengineering (P41EB013598, R01EB016741, R01EB017449), the American Cancer Society (RSG-18-005-01-CCE), the National Cancer Institute (P01CA118816, R01CA183071), and the National Institute of Diabetes and Digestive and Kidney Diseases (R01DK097357, R01DK115987).

Conflicts of interest are listed at the end of this article.

Radiology 2019; 291:273–284 • https://doi.org/10.1148/radiol.2019182391 • Content codes: BQ MR MI

Hyperpolarized (HP) carbon 13 (^{13}C) MRI is an emerging molecular imaging method that allows rapid, noninvasive, and pathway-specific investigation of dynamic metabolic and physiologic processes that were previously inaccessible to imaging. This technique has enabled real-time in vivo investigations of metabolism that are central to a variety of diseases, including cancer, cardiovascular disease, and metabolic diseases of the liver and kidney. This review provides an overview of the methods of hyperpolarization and ^{13}C probes investigated to date in preclinical models of disease. The article then discusses the progress that has been made in translating this technology for clinical investigation. In particular, the potential roles and emerging clinical applications of HP [1-^{13}C] pyruvate MRI will be highlighted. The future directions to enable the adoption of this technology to advance the basic understanding of metabolism, to improve disease diagnosis, and to accelerate treatment assessment are also detailed.

Online supplemental material is available for this article.

Altered metabolism is central to many human diseases, such as cancer, cardiovascular disease, diabetes, and a variety of inflammatory conditions. The most commonly used imaging strategy in the clinic for interrogating metabolism, particularly in cancer, is PET with the glucose analog ^{18}F fluorodeoxyglucose (FDG). FDG PET provides information regarding tissue glucose uptake and has been highly clinically successful. However, it cannot help assess downstream metabolism, which may be useful in the diagnosis and treatment monitoring of a variety of diseases.

Carbon 13 (^{13}C) MRI is particularly attractive for metabolic imaging because carbon serves as the backbone of nearly all organic molecules, thus allowing the investigation of a wide range of biochemical processes that are relevant to human diseases. However, the low natural abundance of the ^{13}C isotope, at 1.1%, has made in vivo imaging extremely challenging. This limitation has been overcome by the recent development of the dynamic nuclear polarization technique, which can dramatically, albeit temporarily, increase the signal of ^{13}C-labeled molecules by more than 10 000 fold (1). Hyperpolarized (HP) ^{13}C MRI has emerged as a powerful molecular imaging strategy that allows safe, nonradioactive, real-time, and pathway-specific investigation of dynamic metabolic and physiologic processes that were previously inaccessible to imaging. In this review, we will provide an overview of the methods of hyperpolarization and the various biologic processes that can be interrogated by using HP ^{13}C probes, with a focus on HP ^{13}C pyruvate. We will also summarize the technical and regulatory requirements of human HP ^{13}C studies and highlight the emerging clinical applications of this molecular imaging technology.

Hyperpolarization

At body temperature and field strengths used in clinical MRI, the MRI signal of ^{13}C endogenous nuclei is very low because of its low natural abundance (only about 1.1% of carbon is ^{13}C) and low nuclear spin polarization (the spins are not well aligned to the external magnetic field). The relative signal of ^{13}C to hydrogen 1 (^{1}H) is 0.016 based on the gyromagnetic ratio of ^{13}C being approximately one-fourth of that of ^{1}H. The relative signal of ^{13}C is further reduced by the low natural abundance of ^{13}C of 1.1%, compared with more than 99% for ^{1}H. To improve the MRI signal of ^{13}C nuclei, probes can be synthetically enriched to increase the concentration of the ^{13}C label in a molecule, commonly enriched to 99% of ^{13}C. MRI signal can be further increased dramatically by the process of hyperpolarization (Fig 1). The principle of hyperpolarization is based on the fact that at low temperature and high magnetic field, electrons have a very high level of polarization (ie, nearly all the electrons are aligned in the same direction). This high level of polarization can be transferred to ^{13}C-labeled probes, increasing their MRI signals. This transfer of polarization is accomplished by mixing radicals (a source of free electrons) with the ^{13}C-labeled probe(s) to be hyperpolarized and placing the mixture in a polarizer at a magnetic field typically of 3.0–5.0 T and at a low temperature (approximately 1 K). Microwave irradiation is then applied to transfer the polarization from unpaired electrons in a trityl radical to the ^{13}C-labeled probes (1). Depending on the molecule to be polarized and the operating field strength and temperature of the

Abbreviations

DHA = dehydroascorbate, FDG = fluorine 18 fluorodeoxyglucose, HP = hyperpolarized, k_{PL} = apparent rate constant for pyruvate-to-lactate conversion, LDH = lactate dehydrogenase, PDH = pyruvate dehydrogenase, TCA = tricarboxylic acid, TRAMP = transgenic adenocarcinoma of mouse prostate

Summary

Hyperpolarized carbon 13 MRI is an emerging molecular imaging technique that is actively undergoing clinical translation at multiple institutions.

Essentials

- Hyperpolarization, achieved by means of dynamic nuclear polarization, dramatically enhances the MRI signal of carbon 13 (^{13}C) labeled molecules by more than 10 000 fold.
- Hyperpolarized ^{13}C MRI allows in vivo probing of enzyme-mediated metabolic processes relevant to human diseases.
- Work is ongoing in the clinical translation of hyperpolarized ^{13}C MRI, with numerous emerging applications in oncology, diabetes, and heart disease, as well as metabolic diseases of the liver and kidney.

polarizer, the hyperpolarization process takes between 30 and 120 minutes. The frozen HP sample is then rapidly dissolved by a heated and pressurized bolus of a biologically compatible buffer solution. The solution retains a high level of polarization and can be formulated to be at physiologic pH, osmolarity, and temperature for in vivo injection and metabolic investigations. In a 3.0-T field and at room temperature, the ^{13}C thermal equilibrium polarization is approximately 0.00025% aligned with the external magnetic field; with hyperpolarization, the polarization increases to approximately 30%–40%, an increase of over 100 000 fold (1), thereby dramatically increasing the MRI signal. The enhanced signal, however, is typically available only for a short period of time (ie, 1–2 minutes), as the polarization decays back to its thermal equilibrium level at a rate dependent on the spin-lattice relaxation time (T1) of the ^{13}C labeled nucleus. Therefore, rapid imaging is needed to acquire high signal-to-noise ratio metabolic data with minimal polarization loss and to measure fast metabolic processes.

HP ^{13}C Probes

An advantage of HP ^{13}C technology is the diverse array of probes that can be polarized. The most commonly studied HP probes have been endogenous biomolecules modified only by the ^{13}C enrichment, and they have been applied to interrogate metabolic and physiologic processes associated with a variety of neoplastic, inflammatory, and metabolic diseases (Table). The selection of the ^{13}C enrichment site should take into account two important considerations. First, the labeled carbon atom should have a long longitudinal relaxation time (T1), as the T1 determines how quickly the polarization of the probe decays back to thermal equilibrium once it is removed from the polarizer. Longer T1 facilitates preservation of the enhanced MRI signal and therefore more accurate quantification of metabolism in vivo. Carbon atoms that do not have directly attached protons, such as those in carbonyl groups, usually have longer T1 relaxation times. Another consideration is the chemical

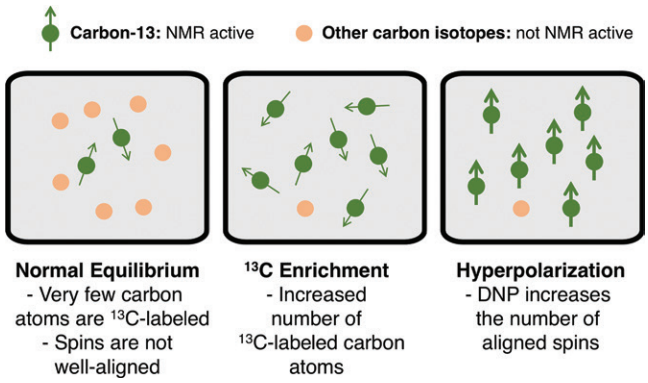

Figure 1: Processes for increasing MRI signal of carbon 13 *(^{13}C)* nuclei. *DNP* = dynamic nuclear polarization, *NMR* = nuclear magnetic resonance.

shift difference between the probe and its metabolites at the labeled position. Larger differences in chemical shift enable differentiation between the probe and metabolites more readily and therefore enable more accurate metabolic quantification. Successful HP probes additionally must be water soluble at physiologic pH values and have cellular uptake that is sufficiently rapid to allow observation of metabolism during the time frame of the HP study.

The most widely studied HP probe to date is [1-^{13}C]pyruvate. It polarizes well (up to 50% polarization level in current clinical polarizers) and has a long T1 (approximately 67 seconds in solution at 3.0 T), thereby permitting in vivo investigation with high signal-to-noise ratio. Importantly, [1-^{13}C]pyruvate is a highly biologically relevant probe, as pyruvate lies at a critical branch point of multiple metabolic pathways, including glycolysis, the tricarboxylic acid (TCA) cycle, and amino acid biosynthesis (Fig 2). On injection into a living system, HP [1-^{13}C]pyruvate is rapidly taken up into the cells and metabolized within the cytosol into [1-^{13}C]lactate and [1-^{13}C]alanine by the enzymes lactate dehydrogenase (LDH) and alanine transaminase, respectively. HP [1-^{13}C]pyruvate is also transported into the mitochondria and is converted by the enzyme pyruvate dehydrogenase (PDH) into ^{13}C CO_2 and acetyl-coenzyme A, thereby serving as a readout of PDH activity and flux toward the TCA cycle. [1-^{13}C]pyruvate has been used extensively to interrogate metabolism in a variety of diseases such as cancer, ischemia, and inflammation in preclinical models (discussed in detail below). Importantly, it has also been translated for clinical metabolic investigations and has been shown to be safe and feasible (2).

There are numerous other HP ^{13}C probes, mainly composed of endogenous biomolecules, that have shown great promise for investigating metabolism relevant to human diseases. Examples include [2-^{13}C]pyruvate for probing mitochondrial metabolism (3,4), [1,4-$^{13}C_2$]fumarate for assessing tissue necrosis (5–9), ^{13}C bicarbonate for measuring pH (10–13), [1-^{13}C]dehydroascorbate (DHA) for interrogating redox capacity (14–18), and ^{13}C urea for imaging perfusion (19–22). While many of these probes have so far been investigated only in preclinical disease models, several of them, including [2-^{13}C]pyruvate, [1,4-$^{13}C_2$]fumarate, and ^{13}C urea are actively being evaluated for clinical translation.

Selected Hyperpolarized Carbon 13 Probes Studied to Date

Probe	Metabolic or Physiologic Processes Interrogated	Applications	T1 (sec)	Chemical Shift (ppm)
[1-^{13}C]pyruvate	Glycolysis; LDH, ALT, PDH activity	Cancer, ischemia, inflammation	67 (At 3.0 T)	[1-^{13}C]pyruvate: 173; [1-^{13}C]lactate: 185; [1-^{13}C]alanine: 178; [1-^{13}C] bicarbonate: 162
[2-^{13}C]pyruvate	TCA cycle metabolism	Cancer, cardiac metabolism	39 (At 3.0 T)	[2-^{13}C]pyruvate: 207.8; [2-^{13}C]lactate: 71; [2-^{13}C]alanine: 53; [5-^{13}C]glutamate: 183.8; [1-^{13}C]acetylcarnitine: 175.2; [1-^{13}C]acetoacetate: 177.3; [3-^{13}C]acetoacetate: 212.7
[1-^{13}C]bicarbonate	pH	Cancer, ischemia	50 (At 3.0 T)	[1-^{13}C]bicarbonate: 161; [1-^{13}C]CO_2: 125
[1,4-$^{13}C_2$]fumarate	Cellular necrosis	Cancer, acute renal tubular necrosis	24 (At 9.4 T)	[1,4-$^{13}C_2$]fumarate: 175.4; [1-^{13}C] malate: 181.8
[5-^{13}C]glutamine	Glutaminase activity, glutamine transport	Cancer	16 (At 9.4 T)	[5-^{13}C]glutamine: 178.5; [5-^{13}C]glutamate: 181.5
[1-^{13}C]dehydroascorbate	Redox	Cancer, diabetes	57 (At 3.0 T)	[1-^{13}C]dehydroascorbate: 174; [1-^{13}C] vitamin C: 177.8
^{13}C urea	Perfusion	Cancer, cardiovascular disease, kidney disease	47 (At 3.0 T)	^{13}C urea: 165
[1-^{13}C]acetate	TCA cycle flux, fatty acid oxidation	Ischemia, cardiac metabolism	40 (At 9.4 T)	[1-^{13}C]acetate: 182.5; [1-^{13}C]AcCoA: 202.1; [1-^{13}C]ALCAR: 174; [5-^{13}C] citrate: 179.7
[1-^{13}C]alpha-ketoglutarate	Mutant IDH expression	Cancer	52 (At 3.0 T)	[1-^{13}C]alpha-ketoglutarate: 172.6; [1-^{13}C]2-HG: 183.9
[2-^{13}C]dihydroxyacetone	Gluconeogenesis	Diabetes	39 (At 3.0 T)	[2-^{13}C]dihydroxyacetone: 213.4; [2–^{13}C]G3P: doublet at 75.0 and 70.4; [2–^{13}C]GA3P: 73.8; [2–^{13}C] PEP: 151.1
[1,3-$^{13}C_2$]acetoacetate	Redox	Cancer, ischemia, diabetes	58 (At 3.0 T)	[1,3-$^{13}C_2$]acetoacetate: 175; [1,3-$^{13}C_2$] βOHB: 180.4

Note.—AcCoA = acetyl-coenzyme A, ALCAR = acetylcarnitine, ALT = alanine transaminase, βOHB = β-hydroxybutyrate, GA3P = glyceraldehyde-3-phosphate, G3P = glycerol-3-phosphate, IDH = isocitrate dehydrogenase, LDH = lactate dehydrogenase, PEP = phosphoenolpyruvate, PDH = pyruvate dehydrogenase, TCA = tricarboxylic acid, 2-HG = 2-hydroxyglutarate.

HP Probes in Preclinical Disease Models

Preclinical studies are critical in testing the feasibility and safety of new HP probes and in developing and refining the methods for their use in specific diseases. In addition, preclinical HP investigations have contributed to our understanding of metabolism and its modification in disease processes and following therapy, thereby yielding important information that is of clinical value. There are more than 50 preclinical polarizers installed worldwide, facilitating a large number of scientific investigations in a variety of diseases.

Cancer

An increase in aerobic glycolysis and lactate production, also known as the Warburg effect, is characteristic of many tumors. Specifically, pyruvate generated from glucose metabolism is preferentially converted to lactate by LDH rather than entering the TCA cycle for oxidative metabolism and adenosine triphosphate generation. This lactate production occurs despite the presence of adequate tissue oxygenation. Hence, HP [1-^{13}C] pyruvate is an ideal probe to noninvasively interrogate such metabolic reprogramming and has been applied to numerous models of cancer (23–33). For example, increased HP [1-^{13}C] pyruvate-to-lactate conversion has been observed in a transgenic adenocarcinoma of mouse prostate (TRAMP) model, with the level of ^{13}C lactate correlating with tumor histologic grade (23) (Fig 3). In a *Myc* oncogene–driven liver cancer model, increased HP [1-^{13}C]pyruvate conversion to lactate and alanine was observed to precede tumor formation, and there was a dramatic reversal of pyruvate-to-lactate conversion during early tumor regression before any size change (24). HP [1-^{13}C]pyruvate–to-lactate conversion and lactate efflux were able to help differentiate benign renal tumors from renal cell carcinomas in an ex vivo model of patient-derived renal tumor tissues (26). These studies have also demonstrated a mechanistic link between HP lactate signal and cellular alterations such as elevated expression of LDH and monocarboxylate transporters (lactate transporters) that are essential to fully understand cancer metabolism.

HP [1-^{13}C]pyruvate has also been shown to be a useful probe to monitor early anticancer therapies. Successful therapies are usually associated with a decrease in pyruvate-to-lactate

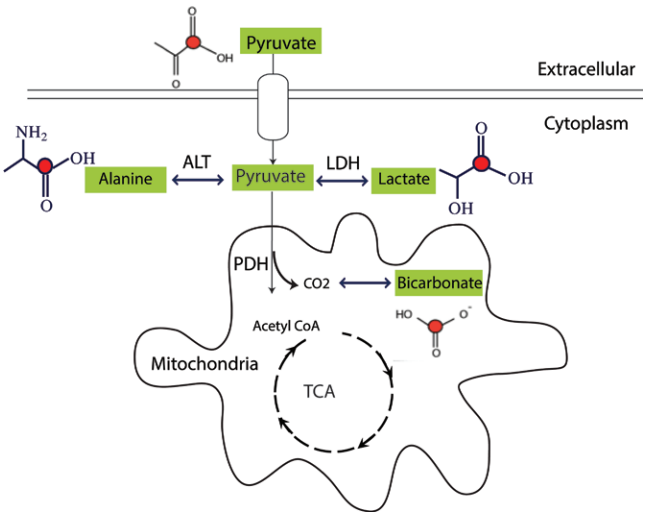

Figure 2: Schematic of the metabolic pathways of pyruvate. [1-^{13}C] pyruvate is rapidly taken up into the cells and metabolized within the cytosol into [1-^{13}C]lactate and [1-^{13}C]alanine by the enzymes lactate dehydrogenase *(LDH)* and alanine transaminase *(ALT)*, respectively. Hyperpolarized [1-^{13}C]pyruvate is also transported into the mitochondria and is converted by the enzyme pyruvate dehydrogenase *(PDH)* into $^{13}CO_2$ and acetyl Co-A, with CO_2 in rapid equilibrium with ^{13}C bicarbonate. *TCA* = tricarboxylic acid. Red circle = position of ^{13}C labeling.

conversion, mediated by different mechanisms from various treatments (34–45). For example, in a model of glioblastoma, decreased lactate production was observed with early treatment response to everolimus (a mammalian target of rapamycin, or mTOR, inhibitor) before any tumor size change and was associated with a decrease in the LDH enzyme that mediates the pyruvate-to-lactate conversion (37). Treatment with temozolomide (a DNA damaging drug) in a glioblastoma model also resulted in lower lactate production but was related to a decrease in pyruvate kinase PKM2, a glycolytic enzyme that indirectly controls pyruvate metabolism (39). Interestingly, in an ovarian cancer model, treatment with a tyrosine kinase inhibitor (pazopanib) led to significantly higher HP pyruvate-to-lactate conversion at 2 days after treatment initiation, while no change was observed at FDG PET (40). The increased pyruvate-to-lactate conversion was hypothesized to reflect increased hypoxia with elevated lactate production as a result of the antiangiogenic effects of the drug (40).

In addition to [1-^{13}C]pyruvate, multiple other probes have been used to study cancer metabolism preclinically. For example, increased HP [1,4-$^{13}C_2$]fumarate–to-malate conversion was seen early following cancer therapy prior to significant changes in tumor size in models of lymphoma (5), breast cancer (46), liver cancer (47), and colon cancer (48), consistent with increased tumor necrosis. Hence, HP fumarate may be useful in providing another measure of early treatment response. HP ^{13}C urea has been used in combination with HP [1-^{13}C]pyruvate to investigate metabolism/perfusion mismatch in a prostate cancer model, and such mismatch was associated with more aggressive tumors (21). A recent study (49) also utilized a combination of [1-^{13}C] pyruvate and HP ^{13}C urea to monitor metabolic and perfusion changes following high-intensity focused ultrasound treatment in a TRAMP model. HP ^{13}C bicarbonate has shown promise for in vivo pH mapping of tumors (10–13,50), which is of great interest, as an acidic tumor microenvironment is implicated in tumor aggressiveness, metastatic potential, and therapeutic response (51).

These initial studies demonstrate the promise of HP ^{13}C MRI in advancing our understanding of cancer metabolism and metabolic response to treatment and, importantly, show the potential of this strategy in detecting early response versus nonresponse, which is critical for enabling adaptive therapies.

Cardiovascular Disease

Alterations in perfusion and energy metabolism are central to many cardiovascular diseases, making them a particularly promising application for HP ^{13}C MRI. Perfusion can be mapped quantitatively by studying the distribution of HP ^{13}C urea (52). Unlike T1-weighted ^{1}H MRI using gadolinium-based perfusion agents, the signal arising from HP ^{13}C urea is linearly dependent on concentration, thus simplifying quantification. Quantitative perfusion mapping with HP ^{13}C urea MRI may be useful in identifying ischemia in patients with balanced hypoperfusion from three-vessel disease, where qualitative gadolinium-enhanced MRI perfusion assessment may be insufficient (53). HP MRI with [1-^{13}C]pyruvate can depict acute changes in myocardial metabolism after ischemia and reperfusion, thereby potentially enabling in vivo monitoring of the metabolic effects of reperfusion strategies (54). Additionally, simultaneous polarization and administration of HP ^{13}C urea and [1-^{13}C]pyruvate permit simultaneous interrogation of cardiac metabolism and perfusion (22). Because HP ^{13}C MRI acquisitions take only 1–2 minutes, this modality has a speed advantage over methods such as PET metabolism/perfusion mismatch studies, where the imaging time approaches 30 minutes. The ability to rapidly assess metabolism/perfusion mismatch and myocardial viability is of clinical relevance in guiding revascularization following acute infarction, in clarifying the functional significance of a perfusion defect, and in guiding treatment selection for patients with angina in the absence of obstructive coronary artery disease.

HP MRI can also help monitor the flux from [1-^{13}C]pyruvate to bicarbonate through the mitochondrial enzyme PDH as a way to examine the relative contribution of glucose and fatty acid oxidation (substrate selection) to energy production in the heart (55–60). In diabetes, the hyperthyroid heart, and dilated cardiomyopathy, flux through PDH in the heart is reduced as measured by HP [1-^{13}C]pyruvate MRI (56–58). In contrast, in hypertrophic cardiomyopathy from hypertension, flux through PDH is increased, indicating a preference for glucose metabolism rather than fatty acid oxidation (60). Other studies have also utilized HP [2-^{13}C]pyruvate MRI to interrogate TCA cycle metabolism during reperfusion and cardiac remodeling following myocardial infarction (61,62). These data show the potential of metabolic profiling with HP ^{13}C MRI as a noninvasive tool to improve understanding of the mechanism of various heart diseases, provide more specific diagnoses, and provide therapeutic guidance.

Liver Disease

A growing body of literature has indicated a strong potential for HP ^{13}C MRI in the diagnosis and monitoring of liver injury

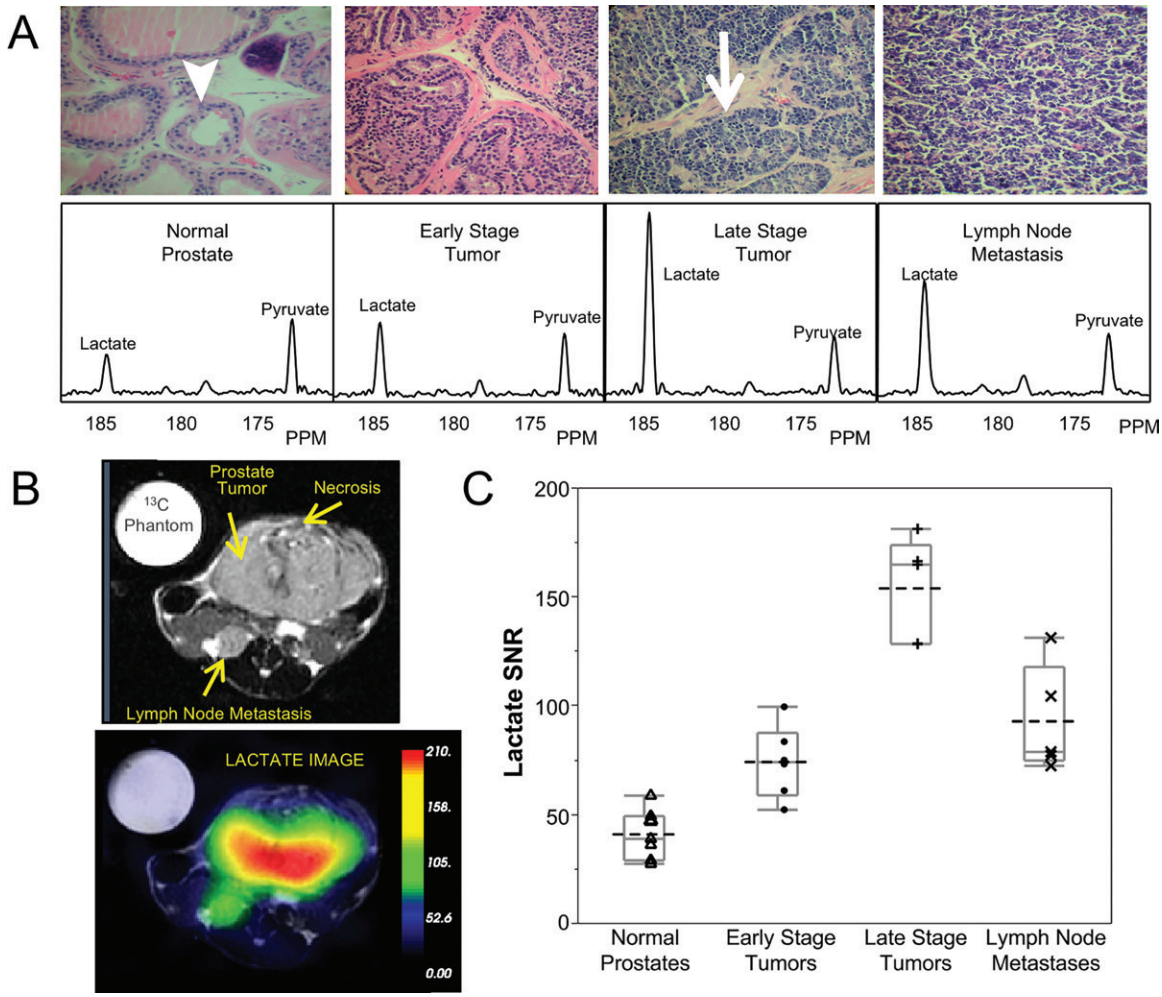

Figure 3: Hyperpolarized (HP) carbon 13 (^{13}C) MRI in a transgenic adenocarcinoma mouse model of prostate cancer. *A,* Representative hematoxylin-eosin–stained pathology sections and HP ^{13}C spectra after injection of HP [1-^{13}C]pyruvate in a normal mouse prostate, an early-stage prostate tumor, a late-stage prostate tumor, and a lymph node metastasis. At histologic examination, normal murine prostate was glandular, with secretory epithelial cells lining the glands (arrowhead). In prostate tumors, there was gradual replacement of the secretory epithelial cells by less differentiated epithelial cells, until the glands were completely eliminated and only anaplastic sheets of pleomorphic cells with irregular nuclei remained in the late stage tumors (arrow). The ^{13}C spectra show an increase in ^{13}C lactate and ^{13}C lactate/pyruvate ratio in late-stage tumor and nodal metastasis. *B,* Axial T2-weighted anatomic MR image and overlay of HP ^{13}C lactate image on T2-weighted image show a qualitatively high level of lactate in a late-stage tumor. Units for color bar = arbitrary units of signal intensity. *C,* Boxplots show quantitative ^{13}C lactate signal in the four histologically defined groups, with late-stage tumors having significantly higher lactate than early-stage tumors. *SNR* = signal-to-noise ratio. (Adapted from reference 23.)

(63–69). For example, increased [1-^{13}C]pyruvate–to-alanine-and-lactate conversion was observed in a model of chemically induced inflammatory liver injury (65), and decreased [1-^{13}C] DHA–to–vitamin C conversion was noted in a model of diet-induced steatohepatitis (18). These results suggest that such an imaging approach may address a currently unmet clinical need for noninvasive diagnosis and treatment monitoring of nonalcoholic steatohepatitis (NASH), a disease of growing concern in the United States and worldwide. HP ^{13}C dihydroxyacetone, a gluconeogenesis precursor, has been used to probe hepatic energy metabolism (68,69), the alteration of which is implicated in both NASH and cirrhosis. To increase the specificity of detected ^{13}C metabolism, a clinically used liver-targeted contrast agent (ie, gadoxetate) can be administered prior to ^{13}C probe injection to selectively suppress the ^{13}C signal from normal hepatocytes (70), as compared with other cell types such as inflammatory cells.

Kidney Disease

In the kidneys, HP ^{13}C MRI has been used to investigate metabolic changes related to hypoxia and oxidative stress (17,71–74), two key factors implicated in progressive kidney injury. Increased renal [1-^{13}C]pyruvate–to-lactate conversion was observed in models of diabetes and has been hypothesized to be related to intrarenal pseudohypoxia from hyperglycemia (71,72). In models of acute kidney injury (ischemia-reperfusion injury), decreased [1-^{13}C]pyruvate–to-bicarbonate conversion has been noted, corresponding to decreased PDH activity and mitochondrial energy production (73,74). The [1-^{13}C]pyruvate–to-

lactate conversion in the injured kidney changes dynamically during the evolution of acute kidney injury (73,74) and may potentially yield information on renal tubular injury during the progression from acute kidney injury to chronic kidney disease. Noninvasive predictors of such progressive kidney injuries are urgently needed given the increasing incidence of chronic kidney disease. The redox probe HP [1-^{13}C]DHA has been shown to sensitively monitor the level of glutathione, a major antioxidant, during progression of diabetes and following treatment targeted to oxidative stress (17). Additionally, the corticomedullary gradient of urea, which is a key osmolyte in the kidney's ability to concentrate urine, can be monitored by using HP ^{13}C urea (75,76), suggesting the potential of this probe to monitor kidney function. While concerns about toxicity have limited the use of gadolinium-based contrast agents in patients with renal insufficiency, HP MRI with endogenous probes such as pyruvate and urea is particularly promising for the noninvasive diagnosis and monitoring of kidney disease.

Inflammation

Chronic inflammation is increasingly recognized as a common factor in many diseases and as a target for therapy. Inflammatory tissues have Warburg-like metabolism and hence can be interrogated by using HP pyruvate MRI. In addition to liver inflammation (as discussed above), increased HP [1-^{13}C]pyruvate–to-lactate conversion has been shown to reflect inflammation in models of radiation-induced lung injury (77), neuroinflammation (78), and inflammatory arthritis (79). Response to anti-inflammatory treatment can similarly be monitored with HP [1-^{13}C]pyruvate MRI (80). Additionally, recent work has explored new HP probes, such as HP [6-^{13}C]arginine (81), that specifically target inflammatory cell metabolism. This is of particular interest in cancer treatment monitoring, as HP [1-^{13}C]pyruvate cannot help differentiate lactate production from cancer cells from that associated with inflammatory cells.

Technical Advances Enabling Clinical Translation of HP ^{13}C MRI

The true potential of HP ^{13}C MRI lies in its rapid progress in clinical translation for patient care. Several technical advances have been made in recent years to achieve this goal. Figure 4 shows the requisite components of human HP ^{13}C studies. These components are explained further below.

Clinical Polarizer

Clinical polarizers are now commercially available (SPINlab; GE Research Circle Technology, Waukesha, Wis) for patient studies (82), with 23 sited around the world. These clinical polarizers allow up to four samples to be polarized at the same time, permitting the injection of multiple probes during a single examination. The preparation of the probes uses a "pharmacy kit," which is filled either in a licensed pharmacy in a sterile compounding environment or by using Good Manufacturing Practice with terminal sterilization following the polarization. The clinical polarizer contains a quality-control module that measures pH, pyruvate and residual radical concentration, polarization, and sample temperature prior to injection to ensure the probe is safe for clinical use. Current clinical polarizers can achieve up to 50% polarization of [1-^{13}C]pyruvate, more than a twofold increase compared with the initial prototype polarizer used for the phase I human study.

Fast Imaging Techniques

The rapid metabolism and relatively short T1 relaxation times of most biologically relevant HP ^{13}C probes have required the development of novel multichannel coil array systems, as well as specialized rapid pulse sequences, and many of these are now commercially available. Multichannel ^{13}C radiofrequency coil arrays allow increased sensitivity and the use of rapid imaging techniques including parallel imaging. For abdominal studies, a commercial 16-channel torso array is available. For other applications, a variety of both custom and commercial ^{13}C MRI coils have been developed with both single-channel receive and multichannel arrays of up to 32 channels for brain tumor studies.

In terms of pulse sequences, two general approaches can be used: a spectroscopic technique and an imaging-based technique. Rapid spectroscopic techniques, such as echo-planar spectroscopic imaging (EPSI), generate a ^{13}C spectrum for every voxel that is imaged (83). These sequences are useful when the exact metabolites are not known, when there are numerous metabolites, or when inhomogeneity in the magnetic field causes the spectral frequencies to be shifted across the sample. In an alternative image-based approach, each metabolite is excited in turn and then imaged by using a conventional imaging sequence such as echo-planar imaging (84), spiral MRI (85), or balanced steady-state free precession (86). The advantage of this approach is that it is faster than EPSI and directly generates images on the MRI unit, which facilitates clinical interpretation. The disadvantages of the imaging-based approaches are that they require the metabolite frequencies to be known beforehand and they are sensitive to nonuniform magnetic fields. To improve the efficient use of HP signal as well as the accuracy and robustness of HP MRI, bolus tracking and real-time B_1 calibration methods have also been implemented recently (87).

Because many metabolic processes are rapid, fast dynamic HP ^{13}C imaging of the substrates and their metabolites is advantageous (88). Dynamic ^{13}C acquisition enables obtaining quantitative metabolic parameters such as the apparent rate constant for pyruvate-to-lactate conversion (k_{PL}), which is less dependent on the precise acquisition and contrast bolus timing. Because the HP ^{13}C signal is nonrenewable, specialized fast imaging strategies are used to conserve magnetization and to allow dynamic data acquisition at multiple time points. For example, compressed sensing reconstruction can be used to minimize the amount of data required. Additionally, special radiofrequency pulses can be used to apply different flip angles to the HP ^{13}C substrates and their metabolites to maximize the signal from the metabolites while preserving the magnetization of the substrates (89).

The MRI unit field strength affects the T1 relaxation time of HP probes. For example, HP ^{13}C pyruvate has slightly shorter T1 at 3.0 T than at 1.5 T. However, the chemical shift separation between pyruvate and its metabolites in hertz at 3.0 T is twice that at 1.5 T; this enables better metabolic quantification. Therefore, current clinical studies of HP ^{13}C pyruvate MRI are commonly performed with 3.0-T MRI units.

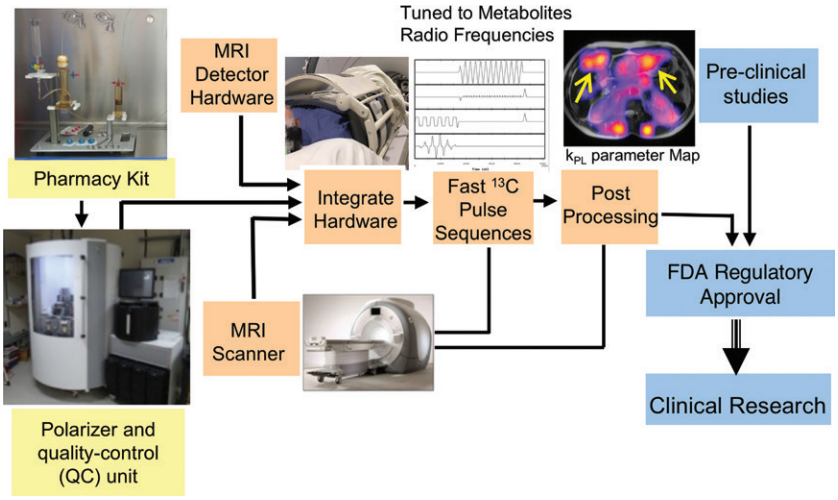

Figure 4: Schematic shows the required components for clinical hyperpolarized carbon 13 (^{13}C) MRI studies. The pharmacy kits used for preparing sterile ^{13}C probes, the clinical polarizers with built-in quality-control units, and specialized MRI detector hardware are now commercially available. Many of the fast ^{13}C pulse sequences and postprocessing tools are available as open source. In the case of [1-^{13}C]pyruvate, the Investigational New Drug resource for its use is available from the National Cancer Institute to assist sites in obtaining U.S. Food and Drug Administration *(FDA)* regulatory approval for clinical HP MRI studies. k_{PL} = apparent rate constant for pyruvate-to-lactate conversion.

Data Analysis

Because HP ^{13}C MRI signal changes rapidly over the course of a study, new approaches for data analysis and quantification are required. One common approach is to express the total signal of downstream metabolites (ie, lactate, alanine) as a fraction of the signal from the injected probe (ie, pyruvate). Alternatively, pharmacokinetic models have been proposed to quantify the apparent rate constants for substrate conversions (2,90–92). For example, k_{PL} can be calculated in patients (92). These approaches need to be further tested and refined in clinical studies to establish the most accurate and reproducible quantitative analysis methods for HP MRI.

Clinical HP Investigations

The two probes [1-^{13}C]pyruvate and [2-^{13}C]pyruvate are currently the probes that have received regulatory approval in the United States (U.S. Food and Drug Administration Investigational New Drug) for clinical investigation. Around the world, 10 sites have performed HP pyruvate MRI in more than 200 human subjects, with several other sites planning clinical studies in the near future. Table E1 (online) lists the up-to-date clinical trials that have registered with *ClinicalTrials.Gov*. These trials are predominantly oncology focused but also include investigations in heart and liver disease and traumatic brain injury, suggesting the potential of this technology for metabolic imaging in a range of human diseases.

Prostate Cancer

The first human study of HP [1-^{13}C]pyruvate MRI was performed in study subjects with localized prostate cancer at the University of California San Francisco and established the safety and feasibility of this new metabolic imaging technique (2). In that study, a dose of up to 0.43 mL [1-^{13}C]pyruvate per kilogram of body weight was administered. Despite being a supra-physiologic level of pyruvate, this dose is rapidly metabolized, and no significant adverse events have been reported to date in clinical studies that used the same dose. In the initial human study, elevated [1-^{13}C]pyruvate–to-lactate conversion was demonstrated in the tumor compared with adjacent normal prostate tissue. In one study subject, elevated lactate signal was seen in a focus of tumor (later confirmed at biopsy) that was not visible on either the T2-weighted or the diffusion-weighted images. These results highlight the potential of this technology to improve tumor detection and characterization. The first results demonstrating metabolic response to androgen deprivation therapy by using HP [1-^{13}C]pyruvate MRI have also been described (93) (Fig 5). After 6 weeks of treatment, there was complete abrogation of the HP ^{13}C lactate signal while there was no change on T2-weighted images and only a modest change on apparent diffusion coefficient maps, illustrating the potential of HP lactate as a biomarker of treatment response. Preliminary data have also demonstrated that HP [1-^{13}C]pyruvate MRI provides reproducible measurements of metabolic changes in the prostates of patients who underwent repeated injections of [1-^{13}C]pyruvate (94). Several other clinical investigations in prostate cancer are currently ongoing, including studies to predict tumor grade in patients before prostatectomy and to assess early treatment response in men with metastatic prostate cancer.

Brain Tumors

In an initial study of eight subjects with a diagnosis of primary brain tumors, HP [1-^{13}C]pyruvate was rapidly transported across the blood-brain barrier and converted to the metabolites lactate and bicarbonate (95) (Fig 6). The non-tumor brain showed high bicarbonate signal that was not detected in the tumors, suggesting that this technique may be valuable for probing mitochondrial oxidative metabolism and its alteration in brain tumors. Another recent study (96) similarly confirmed the feasibility of acquiring high-quality metabolite maps in patients with primary or metastatic brain tumors. These initial clinical studies demonstrated successful technical implementation of HP [1-^{13}C]pyruvate MRI for brain metabolism evaluation. While additional technical optimization is required, the data support further investigation of the clinical utility of this technology in patients with brain tumors, as well as in patients with other neurologic diseases.

Cardiac Metabolism

The first images of HP ^{13}C MRI in the human heart were reported in a pilot study of healthy volunteers (97). The metabolism of [1-^{13}C]pyruvate and the generation of bicarbonate signal in the left ventricular myocardium were visualized with

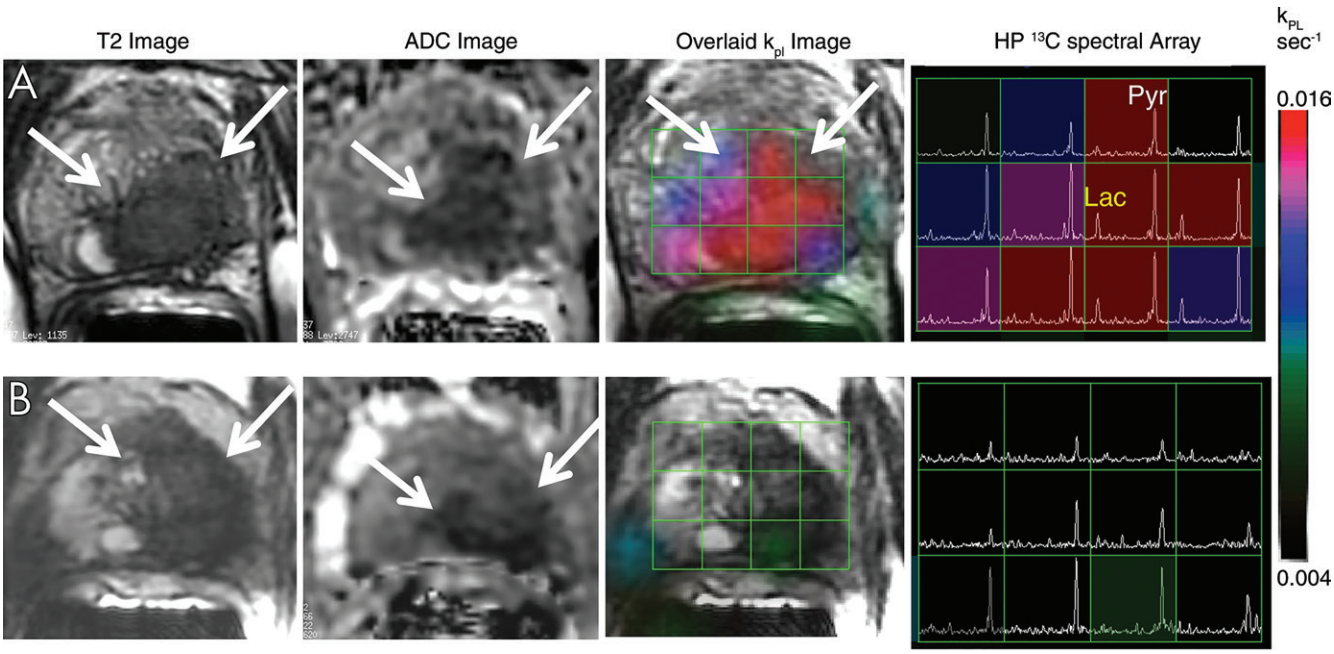

Figure 5: Representative axial T2-weighted MR image, water apparent diffusion coefficient *(ADC)* image, T2-weighted MR image with overlaid apparent rate constant for pyruvate *(Pyr)*-to-lactate *(Lac)* conversion *(k_{PL})*, and corresponding hyperpolarized *(HP)* carbon 13 *(^{13}C)* spectral array in a 52-year-old patient with extensive high-grade (Gleason 4 + 5) prostate cancer, *A,* before therapy and, *B,* 6 weeks after initiation of androgen ablation and chemotherapy. Before treatment, the region of prostate cancer can be seen (arrows) as low signal on the T2-weighted and ADC images, with high HP lactate seen in the spectral array (vertical axis = arbitrary signal intensity units; horizontal axis = frequency in parts per million) and high k_{PL}. At 6 weeks after initiation of androgen deprivation therapy, there was near complete abrogation of elevated HP lactate peaks on the spectral array and associated marked reduction in tumor k_{PL} (maximum k_{PL}, 0.025 sec^{-1} at baseline and 0.007 sec^{-1} at follow-up). Notably, there was negligible change in the size of tumor on T2-weighted MR images and only a modest change on ADC images, supporting the utility of HP [1-^{13}C]pyruvate MRI in detecting early metabolic responses prior to changes on conventional images. Concordant with these findings, the patient subsequently achieved a marked clinical response, with an undetectable serum prostate-specific antigen level 6 months after treatment initiation. (Reprinted, with permission, from reference 91.)

high signal-to-noise ratio. More recently, the same investigators also demonstrated the feasibility of using HP [1-^{13}C]pyruvate to detect metabolic alterations in study subjects with hypertrophic cardiomyopathy (98). Preliminary data showed significantly elevated bicarbonate signal near the cardiac apex, corresponding to the known location of disease. There was also a different spatial distribution of the bicarbonate signal in cardiomyopathy compared with the normal heart. These initial data suggest the exciting possibilities of imaging altered cardiac energetics in patients with heart disease and potentially improving diagnosis and treatment monitoring in these patients.

Other Emerging Applications

In addition to the prostate, brain, and cardiac applications described above, preliminary human results have been obtained in the liver (Fig 7), kidney, pancreas, breast, and bone. As has already been suggested in initial patient data (93), the ability to rapidly monitor response to treatment is likely one of the most promising applications of HP ^{13}C MRI. Particularly in the context of cancer, early detection of nonresponse is essential for minimizing toxicities and redirecting to more effective therapies. Other potential oncologic applications include risk stratification of tumors after the initial diagnosis and determining the most metabolically active region of tumors to target tissue sampling. Furthermore, metabolic changes occurring with diabetes, kidney, and liver disease are also promising areas for exploration in humans.

Comparison with PET

Although FDG PET and HP pyruvate MRI are both sensitive to the metabolic changes that occur in tumors, there are important distinctions that make the two methods complementary. As already discussed, HP MRI with [1-^{13}C]pyruvate provides information at a key branch point of metabolic pathways involved in downstream glucose metabolism—information that is not accessible to FDG PET. For example, prostate cancer often has similar FDG avidity to the background prostate (99). In contrast, a grade-dependent increase in HP pyruvate-to-lactate conversion has been observed in a TRAMP model, as well in patient-derived prostate tissues (23,100), making HP pyruvate MRI a promising tool for assessing tumor aggressiveness. Additionally, FDG PET is sensitive to both glucose uptake and the ability of the cell to trap FDG within cells. For example, some hepatocellular carcinomas have low expression of the glucose transporter GLUT1 but high expression of glucose 6 phosphatase, which phosphorylates FDG and traps it intracellularly, thereby altering the FDG signal (101). Furthermore, because all PET agents produce photons with the same energy, the administered PET probes cannot be distinguished from their products, and it is difficult to image several different PET probes simulta-

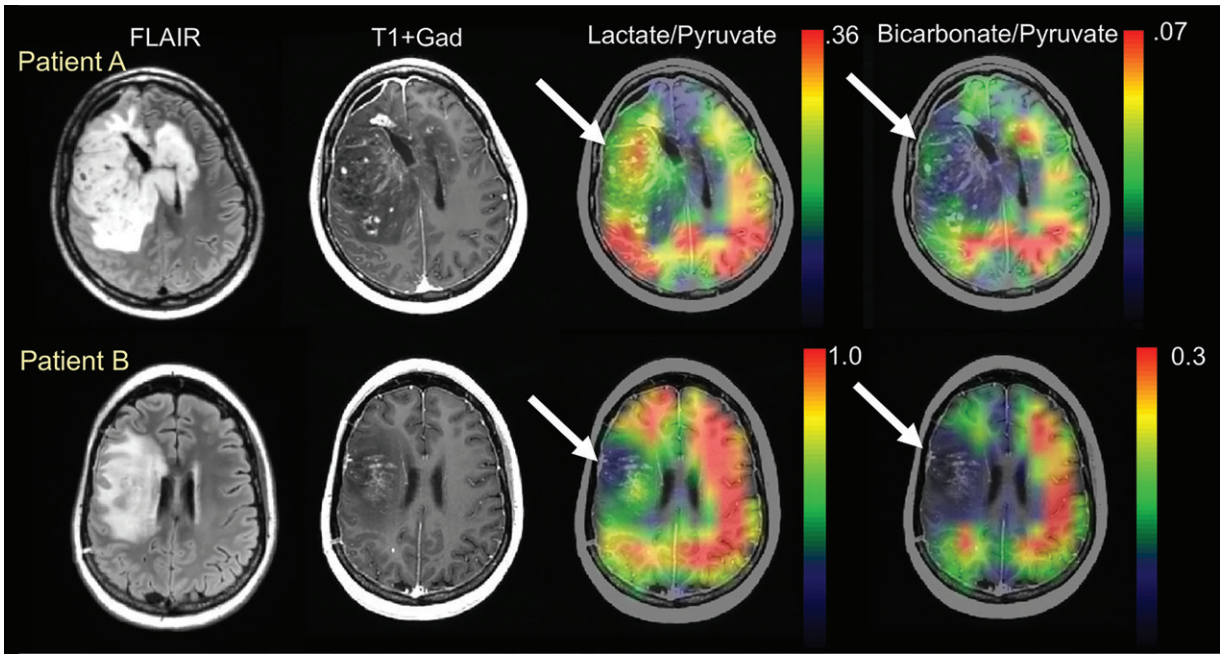

Figure 6: Hyperpolarized (HP) [1-^{13}C]pyruvate MR images in two patients with treated glioblastoma multiforme. Patient A (top row) had progressing tumor at the time of the HP study, while patient B (bottom row) had stable tumor at the time of the HP study. HP [1-^{13}C]pyruvate was rapidly transported across the blood-brain barrier and converted to the metabolites lactate and bicarbonate. There was substantial pyruvate-to-lactate and pyruvate-to-bicarbonate conversion in the normal brain. The tumor (arrows) in patient A, who had progressive tumor, showed moderate pyruvate-to-lactate conversion when compared with normal brain. The tumor (arrow) in patient B, who had clinically stable tumor, showed no substantial pyruvate-to-lactate conversion. Both tumors showed a lack of pyruvate-to-bicarbonate conversion, suggesting reduced mitochondrial oxidative metabolism. Color bars = metabolite ratios. The differences in the scales of the color bars are due to the single-band constant flip angle excitation scheme used for patient A and the multiband variable flip angle excitation scheme used for patient B. These initial findings support the use of HP [1-^{13}C]pyruvate MRI for investigating metabolic reprogramming in brain tumors. *FLAIR* = fluid-attenuated inversion recovery, *Gad* = gadolinium. (Reprinted from reference 93.)

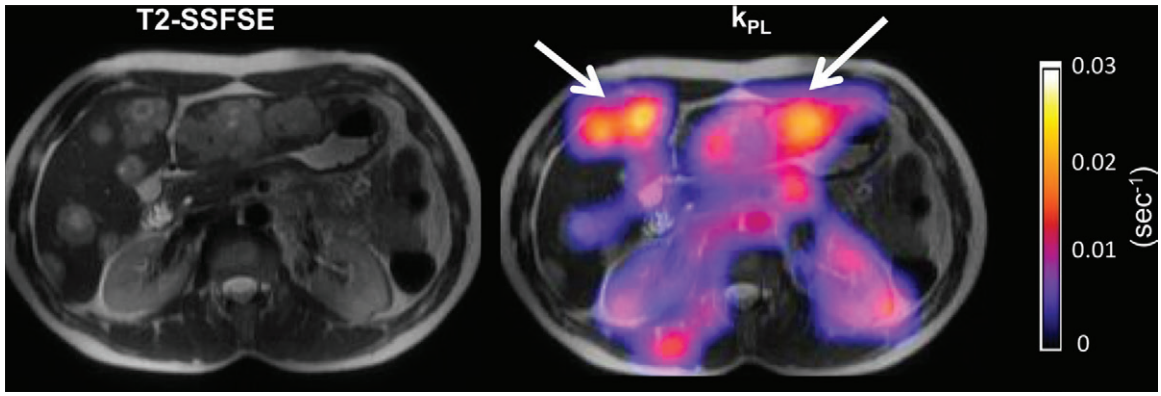

Figure 7: Hyperpolarized (HP) [1-^{13}C]pyruvate MR images in a patient with breast cancer metastatic to the liver. The study was performed by using a 16-channel abdomen carbon 13 (^{13}C) coil array permitting coverage of the whole upper abdomen and a dynamic ^{13}C echo-planar spectroscopic imaging technique at a 2-second time resolution. T2-weighted single-shot fast spin-echo *(SSFSE)* image (left) shows multiple liver metastases. The k_{PL} (the apparent rate constant for pyruvate-to-lactate conversion in sec^{-1}) map overlaid on the T2-weighted SSFSE image (right) shows liver metastases (arrows) with elevated pyruvate-to-lactate conversion, consistent with metabolically active tumors.

neously. In contrast, because HP ^{13}C probes and their metabolites have different resonance frequencies, they can be imaged simultaneously to provide information on multiple metabolic processes (13). Finally, because PET and HP ^{13}C MRI depict complementary aspects of tumor metabolism, it is attractive to explore the combined performance of both modalities. In that context, the advent of the integrated PET/MRI units facilitate such multiparametric examinations.

Challenges and Future Directions

For HP ^{13}C MRI to be adopted as a clinical molecular imaging tool to advance patient care, further efforts are needed in sev-

eral areas. Importantly, these efforts will require a close collaboration between basic scientists and clinicians, as well as a strong partnership between academia, industry, and funding agencies.

Commercially available dual-tuned (^{1}H and ^{13}C) multichannel coils that allow high signal-to-noise ratio imaging for all body areas are essential. Continuing work to improve pulse sequences that permit the imaging of different organs and with different HP ^{13}C probes is necessary to increase clinical applicability. Further refinements are also needed to efficiently and reliably achieve higher and faster polarizations and to simplify methods of sterile HP probe delivery. To facilitate clinical adoption, automated procedures for HP probe delivery, imaging acquisition, and data analysis are also critical.

As indicated in a recent whitepaper (102), Food and Drug Administration approval and clinical adoption of HP ^{13}C MRI will require establishing its clinical utility in subsequent larger phase II and III trials. Critical to this is the demonstration of reproducibility, which will necessitate the establishment of uniform standards for probe production, image acquisition protocol, and data analysis that enable multicenter trials. Early multicenter phase II trials should validate the findings from single-center trials, and indications supported by small multicenter trials can then be carried into larger phase II and phase III studies. These larger trials should not only evaluate safety and efficacy end points but also collect information on clinical impact and cost effectiveness, which are key data for coverage decisions by the Centers for Medicare and Medicaid Services and other payers. In the case of [1-^{13}C]pyruvate, to assist sites planning clinical HP studies, the Investigational New Drug (IND) for the use of [1-^{13}C]pyruvate was transferred to the National Cancer Institute, and the IND resource is available at *https://imaging.cancer.gov/programs_resources/cancer-tracer-synthesis-resources/hyperpolarized-C13-pyruvate-documentation.htm*.

An important consideration in the clinical adoption of HP ^{13}C MRI is cost. The cost of a clinical polarizer is similar to that of a PET cyclotron, and the cost of a Good Manufacturing Practice dose of ^{13}C pyruvate is similar to or less than that of many emerging PET agents. Given the cost, the usage of HP ^{13}C MRI will likely be restricted to large academic medical centers, as in the cases of other high-end imaging technologies. Work is ongoing at multiple institutions to further improve the robustness, reliability, and efficiency of HP ^{13}C MRI (in particular with ^{13}C pyruvate) as a 5-minute add-on to a standard-of-care multiparametric MRI examination. This technology has the potential to provide cost-effective molecular imaging examinations to improve diagnosis and treatment monitoring for various diseases where current imaging methods show limitations.

Conclusions

HP ^{13}C MRI is an emerging molecular imaging technique that is actively undergoing clinical translation at multiple institutions. Preclinical results suggest applications in oncology, diabetes, and heart disease, as well as metabolic disease of the liver and kidney. The tools required for human studies with HP ^{13}C MRI are now commercially available, with clinical trials underway. Further expansion into the clinic will require continued improvement in imaging unit hardware and pulse sequences, formulation of new probes, quantification and standardization of results, and multicenter clinical trials.

Disclosures of Conflicts of Interest: Z.J.W. Activities related to the present article: disclosed no relevant relationships. Activities not related to the present article: holds stock or stock options in Nextrast. Other relationships: disclosed no relevant relationships. **M.A.O.** disclosed no relevant relationships. **P.E.Z.L.** Activities related to the present article: institution received a grant from GE Healthcare. Activities not related to the present article: is on the speakers bureau of GE Healthcare; receives royalties from GE Healthcare, Philips, and Siemens. Other relationships: receives royalties from patents licensed to GE Healthcare. **J.W.G.** disclosed no relevant relationships. **R.A.B.** disclosed no relevant relationships. **J.S.** disclosed no relevant relationships. **J.E.V.** Activities related to the present article: disclosed no relevant relationships. Activities not related to the present article: is a consultant for Medicenna Therapeutics. Other relationships: disclosed no relevant relationships. **C.P.H.** Activities related to the present article: disclosed no relevant relationships. Activities not related to the present article: is on the editorial board of *Radiology*; has been paid for expert testimony by various medicolegal firms; institution has grants or grants pending from General Electric; has been paid for meeting and travel expenses to the Korean Congress of Radiology. Other relationships: disclosed no relevant relationships. **J.K.** disclosed no relevant relationships. **D.B.V.** Activities related to the present article: disclosed no relevant relationships. Activities not related to the present article: institution has received grants for MRI development from GE Healthcare. Other relationships: disclosed no relevant relationships.

References

1. Ardenkjaer-Larsen JH, Fridlund B, Gram A, et al. Increase in signal-to-noise ratio of > 10,000 times in liquid-state NMR. Proc Natl Acad Sci U S A 2003;100(18):10158–10163.
2. Nelson SJ, Kurhanewicz J, Vigneron DB, et al. Metabolic imaging of patients with prostate cancer using hyperpolarized [1-^{13}C]pyruvate. Sci Transl Med 2013;5(198):198ra08.
3. Park JM, Josan S, Grafendorfer T, et al. Measuring mitochondrial metabolism in rat brain in vivo using MR Spectroscopy of hyperpolarized [2-^{13}C] pyruvate. NMR Biomed 2013;26(10):1197–1203.
4. Josan S, Hurd R, Park JM, et al. Dynamic metabolic imaging of hyperpolarized [2-(13) C]pyruvate using spiral chemical shift imaging with alternating spectral band excitation. Magn Reson Med 2014;71(6):2051–2058.
5. Gallagher FA, Kettunen MI, Hu DE, et al. Production of hyperpolarized [1,4-13C2]malate from [1,4-13C2]fumarate is a marker of cell necrosis and treatment response in tumors. Proc Natl Acad Sci U S A 2009;106(47):19801–19806.
6. Mignion L, Dutta P, Martinez GV, Foroutan P, Gillies RJ, Jordan BF. Monitoring chemotherapeutic response by hyperpolarized 13C-fumarate MRS and diffusion MRI. Cancer Res 2014;74(3):686–694.
7. Nielsen PM, Eldirdiri A, Bertelsen LB, Jørgensen HS, Ardenkjaer-Larsen JH, Laustsen C. Fumarase activity: an in vivo and in vitro biomarker for acute kidney injury. Sci Rep 2017;7(1):40812.
8. Clatworthy MR, Kettunen MI, Hu DE, et al. Magnetic resonance imaging with hyperpolarized [1,4-(13)C2]fumarate allows detection of early renal acute tubular necrosis. Proc Natl Acad Sci U S A 2012;109(33):13374–13379.
9. Miller JJ, Lau AZ, Nielsen PM, et al. Hyperpolarized [1,4-$^{13}C_2$]fumarate enables magnetic resonance-based imaging of myocardial necrosis. jacc cardiovasc imaging 2018;11(11):1594–1606.
10. Gallagher FA, Kettunen MI, Day SE, et al. Magnetic resonance imaging of pH in vivo using hyperpolarized 13C-labelled bicarbonate. Nature 2008;453(7197):940–943.
11. Gallagher FA, Sladen H, Kettunen MI, et al. Carbonic anhydrase activity monitored in vivo by hyperpolarized 13C-magnetic resonance spectroscopy demonstrates its importance for pH regulation in tumors. Cancer Res 2015;75(19):4109–4118.
12. Schroeder MA, Swietach P, Atherton HJ, et al. Measuring intracellular pH in the heart using hyperpolarized carbon dioxide and bicarbonate: a 13C and 31P magnetic resonance spectroscopy study. Cardiovasc Res 2010;86(1):82–91.
13. Wilson DM, Keshari KR, Larson PE, et al. Multi-compound polarization by DNP allows simultaneous assessment of multiple enzymatic activities in vivo. J Magn Reson 2010;205(1):141–147.
14. Keshari KR, Kurhanewicz J, Bok R, Larson PE, Vigneron DB, Wilson DM. Hyperpolarized 13C dehydroascorbate as an endogenous redox sensor for in vivo metabolic imaging. Proc Natl Acad Sci U S A 2011;108(46):18606–18611.
15. Bohndiek SE, Kettunen MI, Hu DE, et al. Hyperpolarized [1-13C]-ascorbic and dehydroascorbic acid: vitamin C as a probe for imaging redox status in vivo. J Am Chem Soc 2011;133(30):11795–11801.

16. Keshari KR, Sai V, Wang ZJ, Vanbrocklin HF, Kurhanewicz J, Wilson DM. Hyperpolarized [1-13C]dehydroascorbate MR spectroscopy in a murine model of prostate cancer: comparison with 18F-FDG PET. J Nucl Med 2013;54(6):922–928.
17. Keshari KR, Wilson DM, Sai V, et al. Noninvasive in vivo imaging of diabetes-induced renal oxidative stress and response to therapy using hyperpolarized 13C dehydroascorbate magnetic resonance. Diabetes 2015;64(2):344–352.
18. Wilson DM, Di Gialleonardo V, Wang ZJ, et al. Hyperpolarized ^{13}C spectroscopic evaluation of oxidative stress in a rodent model of steatohepatitis. Sci Rep 2017;7(1):46014.
19. von Morze C, Larson PE, Hu S, et al. Imaging of blood flow using hyperpolarized [(13)C]urea in preclinical cancer models. J Magn Reson Imaging 2011;33(3):692–697.
20. Fuetterer M, Busch J, Peereboom SM, et al. Hyperpolarized ^{13}C urea myocardial first-pass perfusion imaging using velocity-selective excitation. J Cardiovasc Magn Reson 2017;19(1):46.
21. Chen HY, Larson PEZ, Bok RA, et al. Assessing prostate cancer aggressiveness with hyperpolarized dual-agent 3D dynamic imaging of metabolism and perfusion. Cancer Res 2017;77(12):3207–3216.
22. Lau AZ, Miller JJ, Robson MD, Tyler DJ. Simultaneous assessment of cardiac metabolism and perfusion using copolarized [1-^{13} C]pyruvate and ^{13} C-urea. Magn Reson Med 2017;77(1):151–158.
23. Albers MJ, Bok R, Chen AP, et al. Hyperpolarized 13C lactate, pyruvate, and alanine: noninvasive biomarkers for prostate cancer detection and grading. Cancer Res 2008;68(20):8607–8615.
24. Hu S, Balakrishnan A, Bok RA, et al. 13C-pyruvate imaging reveals alterations in glycolysis that precede c-Myc-induced tumor formation and regression. Cell Metab 2011;14(1):131–142.
25. Keshari KR, Sriram R, Koelsch BL, et al. Hyperpolarized 13C-pyruvate magnetic resonance reveals rapid lactate export in metastatic renal cell carcinomas. Cancer Res 2013;73(2):529–538.
26. Sriram R, Van Criekinge M, DeLos Santos J, et al. Non-invasive differentiation of benign renal tumors from clear cell renal cell carcinomas using clinically translatable hyperpolarized ^{13}C pyruvate magnetic resonance. Tomography 2016;2(1):35–42.
27. Golman K, Zandt RI, Lerche M, Pehrson R, Ardenkjaer-Larsen JH. Metabolic imaging by hyperpolarized 13C magnetic resonance imaging for in vivo tumor diagnosis. Cancer Res 2006;66(22):10855–10860.
28. Harris T, Eliyahu G, Frydman L, Degani H. Kinetics of hyperpolarized 13C1-pyruvate transport and metabolism in living human breast cancer cells. Proc Natl Acad Sci U S A 2009;106(43):18131–18136.
29. Hu S, Lustig M, Balakrishnan A, et al. 3D compressed sensing for highly accelerated hyperpolarized (13)C MRSI with in vivo applications to transgenic mouse models of cancer. Magn Reson Med 2010;63(2):312–321.
30. Kettunen MI, Hu DE, Witney TH, et al. Magnetization transfer measurements of exchange between hyperpolarized [1-13C]pyruvate and [1-13C] lactate in a murine lymphoma. Magn Reson Med 2010;63(4):872–880.
31. Park I, Larson PE, Zierhut ML, et al. Hyperpolarized 13C magnetic resonance metabolic imaging: application to brain tumors. Neuro Oncol 2010;12(2):133–144.
32. Park JM, Josan S, Jang T, et al. Metabolite kinetics in C6 rat glioma model using magnetic resonance spectroscopic imaging of hyperpolarized [1-(13) C]pyruvate. Magn Reson Med 2012;68(6):1886–1893.
33. Serrao EM, Kettunen MI, Rodrigues TB, et al. MRI with hyperpolarised [1-13C]pyruvate detects advanced pancreatic preneoplasia prior to invasive disease in a mouse model. Gut 2016;65(3):465–475.
34. Day SE, Kettunen MI, Gallagher FA, et al. Detecting tumor response to treatment using hyperpolarized 13C magnetic resonance imaging and spectroscopy. Nat Med 2007;13(11):1382–1387 [Published correction appears in Nat Med 2007;13(12):1521.] https://doi.org/10.1038/nm1650.
35. Lodi A, Woods SM, Ronen SM. Treatment with the MEK inhibitor U0126 induces decreased hyperpolarized pyruvate to lactate conversion in breast, but not prostate, cancer cells. NMR Biomed 2013;26(3):299–306.
36. Venkatesh HS, Chaumeil MM, Ward CS, Haas-Kogan DA, James CD, Ronen SM. Reduced phosphocholine and hyperpolarized lactate provide magnetic resonance biomarkers of PI3K/Akt/mTOR inhibition in glioblastoma. Neuro Oncol 2012;14(3):315–325.
37. Chaumeil MM, Ozawa T, Park I, et al. Hyperpolarized 13C MR spectroscopic imaging can be used to monitor Everolimus treatment in vivo in an orthotopic rodent model of glioblastoma. Neuroimage 2012;59(1):193–201.
38. Park I, Bok R, Ozawa T, et al. Detection of early response to temozolomide treatment in brain tumors using hyperpolarized 13C MR metabolic imaging. J Magn Reson Imaging 2011;33(6):1284–1290.
39. Park I, Mukherjee J, Ito M, et al. Changes in pyruvate metabolism detected by magnetic resonance imaging are linked to DNA damage and serve as a sensor of temozolomide response in glioblastoma cells. Cancer Res 2014;74(23):7115–7124.
40. Ravoori MK, Singh SP, Lee J, Bankson JA, Kundra V. In vivo assessment of ovarian tumor response to tyrosine kinase inhibitor pazopanib by using hyperpolarized ^{13}C-pyruvate MR spectroscopy and ^{18}F-FDG PET/CT imaging in a mouse model. Radiology 2017;285(3):830–838.
41. Saito K, Matsumoto S, Takakusagi Y, et al. 13C-MR spectroscopic imaging with hyperpolarized [1-13C]pyruvate detects early response to radiotherapy in SCC tumors and HT-29 tumors. Clin Cancer Res 2015;21(22):5073–5081.
42. Day SE, Kettunen MI, Cherukuri MK, et al. Detecting response of rat C6 glioma tumors to radiotherapy using hyperpolarized [1- 13C]pyruvate and 13C magnetic resonance spectroscopic imaging. Magn Reson Med 2011;65(2):557–563.
43. Matsuo M, Kawai T, Kishimoto S, et al. Co-imaging of the tumor oxygenation and metabolism using electron paramagnetic resonance imaging and 13-C hyperpolarized magnetic resonance imaging before and after irradiation. Oncotarget 2018;9(38):25089–25100.
44. Scroggins BT, Matsuo M, White AO, et al. Hyperpolarized [1-^{13}C]-pyruvate magnetic resonance spectroscopic imaging of prostate cancer *In Vivo* predicts efficacy of targeting the Warburg effect. Clin Cancer Res 2018;24(13):3137–3148.
45. Park JM, Spielman DM, Josan S, et al. Hyperpolarized (13)C-lactate to (13)C-bicarbonate ratio as a biomarker for monitoring the acute response of anti-vascular endothelial growth factor (anti-VEGF) treatment. NMR Biomed 2016;29(5):650–659.
46. Witney TH, Kettunen MI, Hu DE, et al. Detecting treatment response in a model of human breast adenocarcinoma using hyperpolarised [1-13C] pyruvate and [1,4-13C2]fumarate. Br J Cancer 2010;103(9):1400–1406.
47. Düwel S, Durst M, Gringeri CV, et al. Multiparametric human hepatocellular carcinoma characterization and therapy response evaluation by hyperpolarized (13) C MRSI. NMR Biomed 2016;29(7):952–960.
48. Bohndiek SE, Kettunen MI, Hu DE, Brindle KM. Hyperpolarized (13)C spectroscopy detects early changes in tumor vasculature and metabolism after VEGF neutralization. Cancer Res 2012;72(4):854–864.
49. Lee JE, Diederich CJ, Bok R, et al. Assessing high-intensity focused ultrasound treatment of prostate cancer with hyperpolarized ^{13} C dual-agent imaging of metabolism and perfusion. NMR Biomed 2018 Jul 18:e3962 [Epub ahead of print] https://doi.org/10.1002/nbm.3962.
50. Scholz DJ, Janich MA, Köllisch U, et al. Quantified pH imaging with hyperpolarized (13) C-bicarbonate. Magn Reson Med 2015;73(6):2274–2282.
51. Estrella V, Chen T, Lloyd M, et al. Acidity generated by the tumor microenvironment drives local invasion. Cancer Res 2013;73(5):1524–1535.
52. Lau AZ, Miller JJ, Robson MD, Tyler DJ. Cardiac perfusion imaging using hyperpolarized (13)C urea using flow sensitizing gradients. Magn Reson Med 2016;75(4):1474–1483.
53. Hagemann CE, Ghotbi AA, Kjær A, Hasbak P. Quantitative myocardial blood flow with Rubidium-82 PET: a clinical perspective. Am J Nucl Med Mol Imaging 2015;5(5):457–468.
54. Oh-Ici D, Wespi P, Busch J, et al. Hyperpolarized metabolic MR imaging of acute myocardial changes and recovery after ischemia-reperfusion in a small-animal model. Radiology 2016;278(3):742–751.
55. Merritt ME, Harrison C, Storey C, Jeffrey FM, Sherry AD, Malloy CR. Hyperpolarized 13C allows a direct measure of flux through a single enzyme-catalyzed step by NMR. Proc Natl Acad Sci U S A 2007;104(50):19773–19777.
56. Schroeder MA, Cochlin LE, Heather LC, Clarke K, Radda GK, Tyler DJ. In vivo assessment of pyruvate dehydrogenase flux in the heart using hyperpolarized carbon-13 magnetic resonance. Proc Natl Acad Sci U S A 2008;105(33):12051–12056.
57. Atherton HJ, Dodd MS, Heather LC, et al. Role of pyruvate dehydrogenase inhibition in the development of hypertrophy in the hyperthyroid rat heart: a combined magnetic resonance imaging and hyperpolarized magnetic resonance spectroscopy study. Circulation 2011;123(22):2552–2561.
58. Schroeder MA, Lau AZ, Chen AP, et al. Hyperpolarized (13)C magnetic resonance reveals early- and late-onset changes to in vivo pyruvate metabolism in the failing heart. Eur J Heart Fail 2013;15(2):130–140.
59. Le Page LM, Rider OJ, Lewis AJ, et al. Increasing pyruvate dehydrogenase flux as a treatment for diabetic cardiomyopathy: a combined 13C hyperpolarized magnetic resonance and echocardiography study. Diabetes 2015;64(8):2735–2743.
60. Dodd MS, Ball DR, Schroeder MA, et al. In vivo alterations in cardiac metabolism and function in the spontaneously hypertensive rat heart. Cardiovasc Res 2012;95(1):69–76.
61. Schroeder MA, Atherton HJ, Ball DR, et al. Real-time assessment of Krebs cycle metabolism using hyperpolarized 13C magnetic resonance spectroscopy. FASEB J 2009;23(8):2529–2538.

62. Dodd MS, Atherton HJ, Carr CA, et al. Impaired in vivo mitochondrial Krebs cycle activity after myocardial infarction assessed using hyperpolarized magnetic resonance spectroscopy. Circ Cardiovasc Imaging 2014;7(6):895–904.
63. Merritt ME, Harrison C, Sherry AD, Malloy CR, Burgess SC. Flux through hepatic pyruvate carboxylase and phosphoenolpyruvate carboxykinase detected by hyperpolarized 13C magnetic resonance. Proc Natl Acad Sci U S A 2011;108(47):19084–19089.
64. Moon CM, Oh CH, Ahn KY, et al. Metabolic biomarkers for non-alcoholic fatty liver disease induced by high-fat diet: in vivo magnetic resonance spectroscopy of hyperpolarized [1-^{13}C] pyruvate. Biochem Biophys Res Commun 2017;482(1):112–119.
65. Josan S, Billingsley K, Orduna J, et al. Assessing inflammatory liver injury in an acute CCl4 model using dynamic 3D metabolic imaging of hyperpolarized [1-(13)C]pyruvate. NMR Biomed 2015;28(12):1671–1677.
66. Moon CM, Shin SS, Lim NY, et al. Metabolic alterations in a rat model of hepatic ischaemia reperfusion injury: in vivo hyperpolarized ^{13} C MRS and metabolic imaging. Liver Int 2018;38(6):1117–1127.
67. Morze CV, Allu PKR, Chang GY, et al. Non-invasive detection of divergent metabolic signals in insulin deficiency vs. insulin resistance in vivo. Sci Rep 2018;8(1):2088.
68. Marco-Rius I, von Morze C, Sriram R, et al. Monitoring acute metabolic changes in the liver and kidneys induced by fructose and glucose using hyperpolarized [2-^{13}C]dihydroxyacetone. Magn Reson Med 2017;77(1):65–73.
69. Moreno KX, Satapati S, DeBerardinis RJ, Burgess SC, Malloy CR, Merritt ME. Real-time detection of hepatic gluconeogenic and glycogenolytic states using hyperpolarized [2-13C]dihydroxyacetone. J Biol Chem 2014;289(52):35859–35867.
70. Ohliger MA, von Morze C, Marco-Rius I, et al. Combining hyperpolarized ^{13} C MRI with a liver-specific gadolinium contrast agent for selective assessment of hepatocyte metabolism. Magn Reson Med 2017;77(6):2356–2363.
71. Laustsen C, Østergaard JA, Lauritzen MH, et al. Assessment of early diabetic renal changes with hyperpolarized [1-(13) C]pyruvate. Diabetes Metab Res Rev 2013;29(2):125–129.
72. Laustsen C, Lycke S, Palm F, et al. High altitude may alter oxygen availability and renal metabolism in diabetics as measured by hyperpolarized [1-(13)C] pyruvate magnetic resonance imaging. Kidney Int 2014;86(1):67–74.
73. Baligand C, Qin H, True-Yasaki A, et al. Hyperpolarized ^{13} C magnetic resonance evaluation of renal ischemia reperfusion injury in a murine model. NMR Biomed 2017;30(10):e3765.
74. Nielsen PM, Laustsen C, Bertelsen LB, et al. In situ lactate dehydrogenase activity: a novel renal cortical imaging biomarker of tubular injury? Am J Physiol Renal Physiol 2017;312(3):F465–F473.
75. Nielsen PM, Szocska Hansen ES, Nørlinger TS, et al. Renal ischemia and reperfusion assessment with three-dimensional hyperpolarized ^{13} C,^{15} N2-urea. Magn Reson Med 2016;76(5):1524–1530.
76. Bertelsen LB, Nielsen PM, Qi H, et al. Diabetes induced renal urea transport alterations assessed with 3D hyperpolarized ^{13} C,^{15} N-Urea. Magn Reson Med 2017;77(4):1650–1655.
77. Thind K, Jensen MD, Hegarty E, et al. Mapping metabolic changes associated with early radiation induced lung injury post conformal radiotherapy using hyperpolarized ^{13}C-pyruvate magnetic resonance spectroscopic imaging. Radiother Oncol 2014;110(2):317–322.
78. Guglielmetti C, Najac C, Didonna A, Van der Linden A, Ronen SM, Chaumeil MM. Hyperpolarized ^{13}C MR metabolic imaging can detect neuroinflammation in vivo in a multiple sclerosis murine model. Proc Natl Acad Sci U S A 2017;114(33):E6982–E6991.
79. MacKenzie JD, Yen YF, Mayer D, Tropp JS, Hurd RE, Spielman DM. Detection of inflammatory arthritis by using hyperpolarized 13C-pyruvate with MR imaging and spectroscopy. Radiology 2011;259(2):414–420.
80. Sriram R, Nguyen J, Santos JD, et al. Molecular detection of inflammation in cell models using hyperpolarized ^{13}C-pyruvate. Theranostics 2018;8(12):3400–3407.
81. Najac C, Chaumeil MM, Kohanbash G, et al. Detection of inflammatory cell function using (13)C magnetic resonance spectroscopy of hyperpolarized [6-(13)C]-arginine. Sci Rep 2016;6(1):31397.
82. Ardenkjaer-Larsen JH, Leach AM, Clarke N, Urbahn J, Anderson D, Skloss TW. Dynamic nuclear polarization polarizer for sterile use intent. NMR Biomed 2011;24(8):927–932.
83. Chen HY, Larson PEZ, Gordon JW, et al. Technique development of 3D dynamic CS-EPSI for hyperpolarized ^{13} C pyruvate MR molecular imaging of human prostate cancer. Magn Reson Med 2018;80(5):2062–2072.
84. Gordon JW, Vigneron DB, Larson PE. Development of a symmetric echo planar imaging framework for clinical translation of rapid dynamic hyperpolarized ^{13} C imaging. Magn Reson Med 2017;77(2):826–832.
85. Lau AZ, Chen AP, Ghugre NR, et al. Rapid multislice imaging of hyperpolarized 13C pyruvate and bicarbonate in the heart. Magn Reson Med 2010;64(5):1323–1331.
86. Milshteyn E, von Morze C, Gordon JW, Zhu Z, Larson PEZ, Vigneron DB. High spatiotemporal resolution bSSFP imaging of hyperpolarized [1-^{13} C]pyruvate and [1-^{13} C]lactate with spectral suppression of alanine and pyruvate-hydrate. Magn Reson Med 2018;80(3):1048–1060.
87. Tang S, Jiang W, Chen HY, Bok R, Vigneron DB, Larson PEA. A 2DRF pulse sequence for bolus tracking in hyperpolarized 13C imaging. Magn Reson Med 2015;74(2):506–512.
88. Golman K, in 't Zandt R, Thaning M. Real-time metabolic imaging. Proc Natl Acad Sci U S A 2006;103(30):11270–11275.
89. Larson PE, Hu S, Lustig M, et al. Fast dynamic 3D MR spectroscopic imaging with compressed sensing and multiband excitation pulses for hyperpolarized 13C studies. Magn Reson Med 2011;65(3):610–619.
90. Bankson JA, Walker CM, Ramirez MS, et al. Kinetic modeling and constrained reconstruction of hyperpolarized [1-13C]-pyruvate offers improved metabolic imaging of tumors. Cancer Res 2015;75(22):4708–4717.
91. Harrison C, Yang C, Jindal A, et al. Comparison of kinetic models for analysis of pyruvate-to-lactate exchange by hyperpolarized 13 C NMR. NMR Biomed 2012;25(11):1286–1294.
92. Larson PEZ, Chen HY, Gordon JW, et al. Investigation of analysis methods for hyperpolarized 13C-pyruvate metabolic MRI in prostate cancer patients. NMR Biomed 2018;31(11):e3997.
93. Aggarwal R, Vigneron DB, Kurhanewicz J. Hyperpolarized 1-[^{13}C]-pyruvate magnetic resonance imaging detects an early metabolic response to androgen ablation therapy in prostate cancer. Eur Urol 2017;72(6):1028–1029.
94. Granlund KL, Vargas HA, Lyashchenko SK, et al. Utilizing hyperpolarized MRI in prostate cancer to assess metabolic dynamics and histopathologic grade [abstr]. In: Proceedings of the Twenty-Fifth Meeting of the International Society for Magnetic Resonance in Medicine. Berkeley, Calif: International Society for Magnetic Resonance in Medicine, 2017; 0727.
95. Park I, Larson PEZ, Gordon JW, et al. Development of methods and feasibility of using hyperpolarized carbon-13 imaging data for evaluating brain metabolism in patient studies. Magn Reson Med 2018;80(3):864–873.
96. Miloushev VZ, Granlund KL, Boltyanskiy R, et al. Metabolic imaging of the human brain with hyperpolarized ^{13}C pyruvate demonstrates ^{13}C lactate production in brain tumor patients. Cancer Res 2018;78(14):3755–3760.
97. Cunningham CH, Lau JY, Chen AP, et al. Hyperpolarized 13C metabolic MRI of the human heart: initial experience. Circ Res 2016;119(11):1177–1182.
98. Lau AZ, Chen AP, Lau JY, et al. Hyperpolarized 13C metabolic imaging of human hypertrophic cardiomyopathy [abstr]. In: Proceedings of the Twenty-Sixth Meeting of the International Society for Magnetic Resonance in Medicine. Berkeley, Calif: International Society for Magnetic Resonance in Medicine, 2018; 0276.
99. Salminen E, Hogg A, Binns D, Frydenberg M, Hicks R. Investigations with FDG-PET scanning in prostate cancer show limited value for clinical practice. Acta Oncol 2002;41(5):425–429.
100. Keshari KR, Sriram R, Van Criekinge M, et al. Metabolic reprogramming and validation of hyperpolarized 13C lactate as a prostate cancer biomarker using a human prostate tissue slice culture bioreactor. Prostate 2013;73(11):1171–1181.
101. Izuishi K, Yamamoto Y, Mori H, et al. Molecular mechanisms of [18F]fluorodeoxyglucose accumulation in liver cancer. Oncol Rep 2014;31(2):701–706.
102. Kurhanewicz J, Vigneron DB, Ardenkjaer-Larsen JH, et al. Hyperpolarized ^{13}C MRI: path to clinical translation in oncology. Neoplasia 2019;21(1):1–16.